This is the accepted version of the article (+SI) published in the final form in
Chemistry A European Journal, e202201969, 2022
by Wiley-VCH GmbH
DOI: 10.1002/chem.202201969.
https://doi.org/10.1002/chem.202201969

Efficient water cleaning by self-standing carbon nitride films derived from supramolecular hydrogels

Junyi Li,[a] Snir Dor,[b] Jesús Barrio,*[c] and Menny Shalom*[a]

[a] J. Li, Prof. M. Shalom
Department of Chemistry and Ilse Katz Institute for Nanoscale Science and Technology
Ben-Gurion University of the Negev
Beer-Sheva 8410501, Israel
E-mail: mennysh@bgu.ac.il
[b] S. Dor
Department of Materials Engineering
Israel Ministry of Defense
Hakirya, Tel Aviv 61909, Israel
[c] Dr. J. Barrio
Department of Materials, Royal School of Mines
Imperial College London
London SW72AZ, England, UK
Email: j.barrio-hermida@imperial.ac.uk

Abstract: The design of efficient self-standing hybrid systems for water purification that combines good adsorption properties with high photodegradation ability is highly challenging owing to the difficulty in simultaneously controlling the band structure and porosity of a semiconductor while maintaining its self-standing nature. Here, we report the synthesis of carbon-rich carbon nitride self-standing filters from supramolecular hydrogels composed of melamine and cyanobenzoic acid. The influence of the chemical structure on the properties of the hydrogels and the final films was studied by tuning parameters such as monomer nature, molar ratio, and pyrolysis temperature. Thanks to their ability to combine the adsorption and photodegradation of organic pollutants, the prepared self-standing films showed remarkable activity and stability in flow conditions (>95% efficiency after 10 consecutive cycles). Additionally, the photocatalytic activity of the films was assessed in the powder form for the hydrogen evolution reaction and photocurrent generation in a photoelectrochemical cell. The reported work opens opportunities for the controlled synthesis of multifunctional filters for water purification and other energy-related and sustainable technologies.

Introduction

Water pollution has emerged as one of the major challenges of modern society within the last decades, owing to the rise in world population and the waste generated from extensive agriculture.[1] Wastewater treatment technologies, which remove pollutants and provide clean water in areas with limited supply, are therefore sought after. Achieving such an aim requires the careful engineering of membrane materials that can adsorb those pollutants within their porous hierarchical structure or decompose them via photocatalysis.[2] Currently, membrane technologies relying on filtration to remove contaminants are one of the most commonly applied processes for wastewater treatment.[3,4] Porous materials such as activated carbon,[5] zeolites,[6] or boron nitride[7] have emerged as effective adsorbents for water cleaning. However, the development of porous semiconductor materials that can simultaneously adsorb and degrade contaminants remains in its infancy. [8,9]
The removal of pollutants through heterogeneous photocatalytic processes consists of generating highly reactive and non-selective hydroxyl and superoxide anion radicals on the surface of a semiconductor photocatalyst, which then attack and decompose organic molecules.[10] Therefore, the design of hybrid systems combining membrane filtration with photodegradation offers great prospects for the removal of pollutants from wastewater.
Recently, polymeric carbon nitride materials have attracted considerable attention as photocatalysts, owing to their suitable optical band gap, low cost, and high thermal and chemical stability.[11–14] The photocatalytic activity of particulate carbon nitride materials has been extensively studied for processes such as hydrogen generation from water,[15–18] CO_2 reduction,[19–22] water oxidation,[23–25] organic transformations,[26–29] and pollutants degradation.[30–32] However, the lack of solubility arising from interplanar Van der Waals interactions in carbon nitride materials hinders their application in advanced devices that require self-standing thin films. Consequently, there has been a growing interest in developing novel synthetic approaches that can provide efficient photoactive carbon nitride self-standing materials.[33,34] To date, supported carbon nitride films have often been obtained by the direct pyrolysis of a C-N based building block or supramolecular precursor on a given substrate.[35,36] Xiao et al. prepared free-standing polymeric carbon nitride membranes through vapor-deposition polymerization, which then exhibited excellent photo-driven ionic transport properties.[37,38] Self-standing carbon nitride films have been mostly obtained by photopolymerization in the presence of suitable cross-linkers,[39,40] or by self-assembly with other nanomaterials such as polyoxometalates. [41] To overcome this problem, in this work, we prepared carbon nitride self-standing films by the pyrolysis at high temperatures of tailored supramolecular hydrogels based on melamine and 4-cyanobenzoic acid. Previous research has shown that in the presence of carboxylic acids, melamine can form unique supramolecular synthons that include solvent molecules within their crystal structure.[42–44] These supramolecular architectures can impart hierarchical porosity and self-standing capability to the carbon nitride materials resulting from their pyrolysis, making them suitable as self-standing filters for water purification.[45] The obtained films were tested as water-cleaning filters in a continuous hybrid process involving physical adsorption and photodegradation, showing remarkable performance in the degradation of rhodamine B and methylene blue dyes. Additionally, the

synthetic approach was expanded to a various of C-N based monomers.

Results and Discussion

The supramolecular CBMA precursors were prepared by dissolution of 4-cyanobenzoic acid (CB) and melamine (MA) at different molar ratios in hot distilled water, followed by slow evaporation of the solvent (Scheme 1). As shown in Figure 1a, a white bulk precursor hydrogel is obtained once the solution has cool down to room temperature, with a shape determined by the mold employed. This hydrogel can then be converted into a xerogel after solvent removal, still maintaining its original shape. Castiñeiras and co-workers observed that protonated melamine forms a one-dimensional ribbon through linear N–H···N hydrogen bonds in the presence of carboxylic acids such as mandelic and glycolic acid, which form anionic dimers connected through O–H···O hydrogen bonds.[42] We hypothesize that upon interaction with CB and water molecules, protonated melamine forms a 3D arrangement involving in-plane hydrogen bonds (N-H···N between melamine residues and N-H···O with CB molecules) and π–π stacking interactions (Scheme 1).[46]

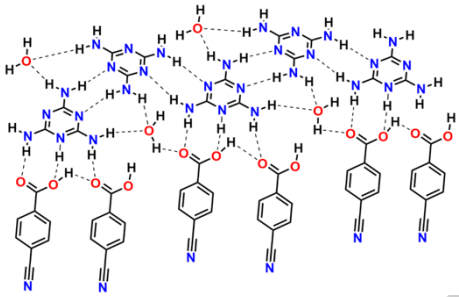

Scheme 1. Suggested structure for the supramolecular assembly formed in water between melamine and 4-cyanobenzoic acid.

X-ray diffraction (XRD) and Fourier transform infrared spectroscopy (FTIR) were used to examine the formation of supramolecular structures. As shown in Figure 1b, in the XRD pattern of CBMA, the diffraction peaks corresponding to CB and MA are significantly weakened or even disappear, and a different pattern is observed corresponding to the formation of a new supramolecular periodic structure.[47] Furthermore, whereas the peak intensities for the cyano (2220 cm^{-1}) and carbonyl groups (1675 cm^{-1}) remain about the same, the peaks arising from the stretching vibration of the amine groups of melamine (3000-3500 cm^{-1}) and the hydroxyl functionality of cyanobenzoic acid (1210-1350 cm^{-1}) partially vanish because of the involvement of hydroxyl groups in the hydrogen-bonded framework (Figure 1c). Scanning electron microscopy (SEM) images (Figure 1d and Figure S1) show the rod morphology of this supramolecular precursor.

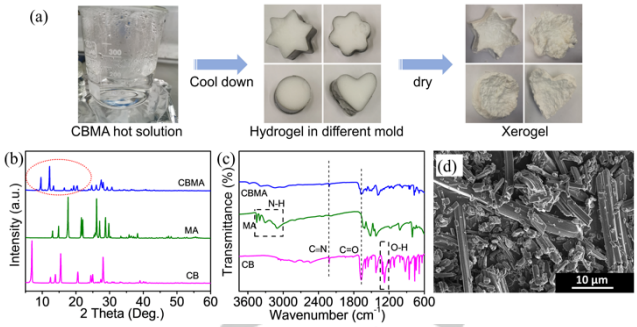

Figure 1. Figure Caption. Figure 1. (a) Preparation of CBMA hydrogels and xerogels. (b) XRD patterns, (c) FTIR spectra, and (d) SEM image of supramolecular precursor CBMA (1:1 ratio).

The effect of the chemical composition on the structure of the supramolecular self-assembly was studied through variations of the starting CB/MA ratio. As the proportion of CB is increased, the intensity of the XRD peaks of melamine gradually weakens, and new diffraction peaks corresponding to the supramolecular aggregate emerge. When the CB/MA ratio is 1, the melamine diffraction peaks completely disappear (Figure S2), suggesting the formation of a stoichiometric arrangement. This hypothesis is supported by the FTIR spectra of CBMAs (Figure S2), where the amino group vibration peak at 3449 cm^{-1} gradually vanish when approaching the 1 :1 stoichiometry. These results indicate that at a CB/MA ratio of 1, the assembly of the supramolecular structure is complete, and no excess of either of the monomers remains. Furthermore, SEM images (Figure S3) show that the average particle size substantially increases with the CB/MA ratio.

In order to study this synthetic approach with a wider variety of precursors, thereby showing its applicability to the synthesis of different materials, we replaced melamine with other precursors commonly employed in the preparation of photoactive polymers, namely urea,[48] dicyandiamide (DCD),[49] acetoguanamine (AGA),[50,51] and 2,4,6-triaminopyrimidine (TAP),[52,53] and we studied the supramolecular self-assembly behavior of the resulting mixture. Amongst those monomers, we observed that only TAP was able to form a bulk hydrogel with cyanobenzoic acid, probably owing to the very similar structure and hydrogen-bonding ability of TAP and MA.[46,54] FTIR spectra (Figure S4) show that the C–OH vibrational modes (1210-1350 cm^{-1}) in CBMA, CBTAP and CBAGA are significantly weakened, which can be ascribed to the formation of supramolecular structures through hydrogen bonding. However, these vibrations remain unchanged in CB-urea, CBDCD, and pure CB, which suggests that the protonated N groups on the six-membered ring play an important role in the self-assembly, including by strengthening π–π stacking interactions.[55]

The supramolecular precursors were pyrolyzed at different temperatures to prepare porous, self-standing carbon nitride materials. After pyrolysis of CBMA, robust, lightweight thin films were obtained (Figure 2). SEM images (Figure 2) show an interconnected hierarchically porous structure, and nitrogen sorption isotherms reveal BET surface areas of 18, 23, and 35 $m^2\ g^{-1}$ for CBMA500, CBMA550, and CBMA600, respectively (Figure S5).

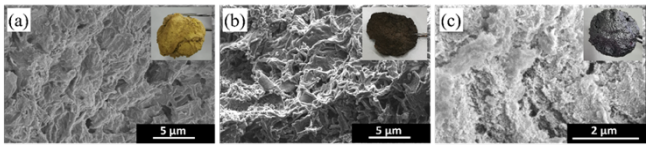

Figure 2. SEM images of as-obtained CBMA samples synthesized at different temperatures. (a) 500 °C (CBMA500), (b) 550 °C (CBMA550), and (c) 600 °C (CBMA600). The inserts contain a digital image of the analyzed films.

XRD patterns (Figure S6) of the samples synthesized at different temperatures all show clear diffraction peaks at 2θ values of 27° and 13°, which respectively arise from the characteristic interplanar stacking of conjugated aromatic units (indexed as (002) plane) and the in-plane triazine motif of graphitic carbon nitride, indexed as (100). The (002) plane is slightly shifted from 26.8 to 27.3° with higher reaction temperatures, which corresponds to a change in interplanar distance from 0.332 to 0.326 nm. We observed that at higher pyrolysis temperatures, the (100) diffraction peak vanishes; we attribute this to the partial decomposition of carbon nitride at higher temperatures, which leads to a more disordered in-plane structure. Additionally, FTIR analysis (Figure S6b) further proves the formation of polymeric entities: all the materials display bands at 2900-3500 cm^{-1}, which can be assigned to N-H vibrational modes, strong peaks between 1200-1700 cm^{-1} associated with stretching vibrations of triazine rings, and a sharp peak at 806 cm^{-1} corresponding to the breathing vibration of the triazine group.[30]

X-ray photoelectron spectroscopy (XPS) and elemental analysis (EA) were carried out to further reveal the chemical composition and chemical state of the elements within the obtained materials. As shown in Figure S7, the XPS survey spectra of all samples show the presence of C, N, and O elements. Hydrogen coming from –NH moieties in the grain boundaries is also observed through EA (Table S1); the overall content decreases at higher pyrolysis temperatures, owing to the lower number of –NH species. In addition, the C/N ratio increases significantly when the reaction temperature reaches 600 °C, which can be ascribed to the release of nitrogen species and subsequent formation of vacancies at such temperatures.[56] Of note, the resulting carbon nitride materials had a higher C/N ratio and oxygen content than the conventional materials of the state of the art, owing to the preservation of structural carbon and oxygen from CB in the supramolecular hydrogels. The high-resolution C1s spectra can be deconvoluted into three different chemical binding energies (Figure S6c) at 284.8, 286.0, and 288.2 eV, respectively corresponding to sp^2 C–C within the structure and adventitious carbon, C–O bonds, and sp^2-hybridized carbon bonded to nitrogen within the triazine ring (N–C=N). We observed that the N–C=N contribution decreases significantly when the employed reaction temperature is 600 °C, owing to partial degradation of the carbon nitride framework, as suggested by elemental analysis. In the N 1s XPS spectra, four peaks at 398.4, 399.0, 400.3, and 401.3 eV were identified (Figure S6d), corresponding to sp^2-hybridized nitrogen in triazine rings (C-N=C), bridging N atoms in N-$(C)_3$ groups, amino groups (N-H), and oxidized N (NO_x).

Optical properties studies (Figure 3a) indicate a red-shifted adsorption edge and enhanced visible light absorption at higher calcination temperatures, in agreement with the observed color of the samples. The Tauc plots (Figure S8) of CBMA500, CBMA550, and CBMA600 reveal optical band gaps of 1.9 eV, 1.7 eV, and 1.6 eV, respectively—substantially narrower than that of conventional carbon nitride (2.7 eV). The flat band potentials shown at Figure S9-10 (Determined by Mott-Schottky electrochemical measurements [57-58]) indicate that the prepared materials display a conduction band negative enough to drive the hydrogen evolution reaction. The charge separation efficiency of the photogenerated electron–hole pairs of the as-obtained samples was studied by measuring the generated photocurrent in a standard water-splitting photoelectrochemical cell. As shown in Figure 3b, the photocurrent density of CBMA550 at 1.23 V vs RHE reaches up to 20 µA cm^{-2}, higher than that of the materials prepared at 500 and 600 °C, implying a better charge separation efficiency.

The self-standing nature and hierarchical porosity of the prepared films make them suitable candidates as membranes for the adsorption of contaminants from water. Therefore, the adsorption capacity of the as-prepared carbon nitride films for a model pollutant was studied by adding CBMA500 into an aqueous solution of methylene blue (MB) and spectrophotometrically analyzing the equilibrium concentration of MB at different time intervals. The adsorption isotherms were simulated non-linear forms of Langmuir and Freundlich models (Figure 3c). The calculated adsorption parameters and correlation coefficients (R^2) based on Langmuir and Freundlich models are given in Table S2. The n values in the Freundlich model range from 2.46 to 3.71, suggesting that the analyzed carbon nitride materials have a good ability to adsorb MB. The R^2 values of the Langmuir model fits are >95% for all samples (higher than those of the Freundlich model), suggesting that the Langmuir model is more accurate than the Freundlich model. Therefore, the Langmuir model was applied to calculate the adsorption capacity (Q_0 value) of samples prepared at different reaction conditions. They follow the order: CBMA600 (3.28 mg g^{-1}) > CBMA550 (2.61 mg g^{-1}) > CBMA500 (2.11 mg g^{-1}) > B-CN (1.32 mg g^{-1}), which shows a good correlation with their specific surface areas.

To test the prepared materials in a hybrid water cleaning system, we initially evaluated the photoactivity of as-prepared samples in the hydrogen evolution reaction from water with Pt as co-catalyst and in the degradation of MB. For such experiments, as-obtained samples were ground and employed as dispersed powder photocatalysts. As shown in Figure 3d and Figure S11-12, CBMA550 exhibits the highest photocatalytic hydrogen evolution rate and MB degradation rate; these rates are consistent with the trend in photocurrent density generation rather than with the trend in specific surface area, indicating that the photocatalytic performance is limited by charge separation rather than mass transfer.

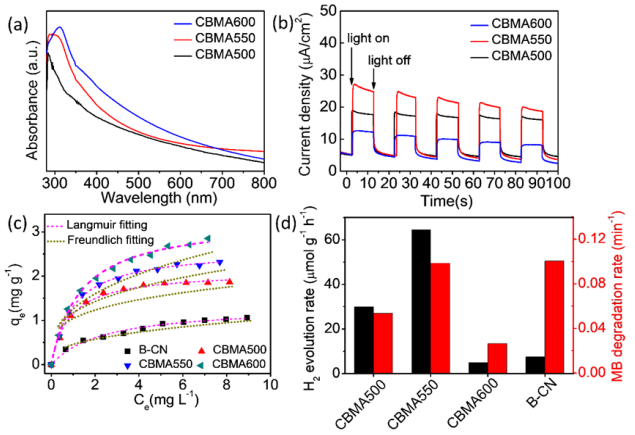

Figure 3. (a) UV–vis absorption spectra, (b) transient photocurrent responses, (c) adsorption performance for MB, and (d) photocatalytic activities of as-obtained carbon nitride samples.

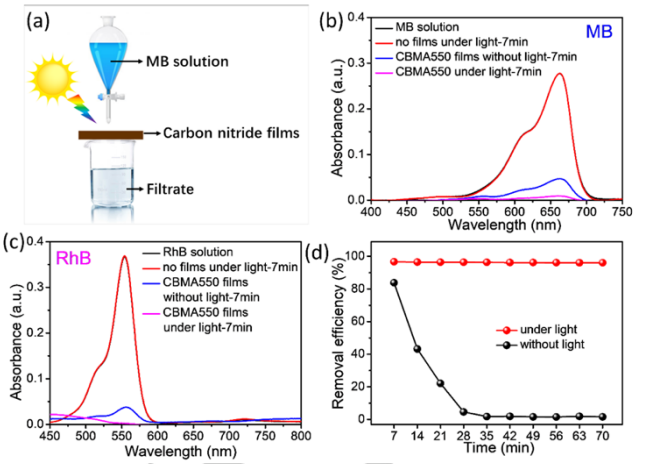

Figure 4. (a) Schematic diagram of filtration and photodegradation process. UV-vis absorbance spectra of filtrate from (b) MB and (c) RhB solutions. (d) Removal efficiency of MB as a function of time for solutions passed through CBMA550 films.

Given the adsorption and photodegradation capabilities of the self-standing materials, we studied their water-cleaning performance in a more realistic configuration by analyzing the in situ removal of dyes from water under a constant flow. The as-obtained carbon nitride films were therefore used as photomembranes combining filtration and photodegradation for the removal of pollutants from wastewater. A schematic of the photodegradation setup is shown in Figure 4a. Permeation flux studies were carried out by filtering 5 mL MB aqueous solution in a CBMA550 membrane of 2 cm^2 and 1 mm thick while recording the filtration time. A water permeation flux of 213 L h^{-1} m^{-2} and a removal efficiency of 83.8 % were achieved for CBMA550 film. Additionally, to study the impact of film thickness on the water permeation, CBMA550 films of different thickness were prepared by tuning the size of precursors. 0.5 mm and 2 mm thick films displayed water permeation flux of 336 L h^{-1} m^{-2} and 134 L h^{-1} m^{-2}, with removal efficiencies of 76.8% and 89.4%, respectively. It is reasonable that thinner films have higher water permeation flux and lower adsorption capacities. 1 mm thick CBMA550 films were selected on account of their suitable permeation flux and superior adsorption properties. A 20 mg L^{-1} MB (or Rhodamine B, RhB) aqueous solution was deposited dropwise (0.714 mL min^{-1}) on the filter membrane under continuous illumination. After 7 min, the filtrate was transferred into a UV-vis spectrophotometer to determine the dye concentration. As shown in Figure 4b-c, by combining filtration and photodegradation for 7 min (during which 5 mL of dye solution passed through the membrane), the CBMA550 films exhibited excellent dye treatment efficiency for both MB and RhB solutions.

After 7 min, the removal efficiency for MB and RhB was as high as 96% and 97%, respectively. To obtain further insights into the stability and recyclability of the membrane, we conducted continuous MB degradation experiments using 7 min cycles; the filtrate was transferred into a spectrophotometer to determine the dye concentration after each cycle (Figure S13). The removal efficiency for each cycle, under light and without light, is shown in Figure 4d: the CBMA550 films retained excellent removal efficiency and stability after 70 min under light irradiation (i.e., after the whole 50 mL dye solution was passed), whereas in darkness, the filter was saturated after roughly 30 min and was not able to adsorb any more MB.

Conclusion

In summary, we prepared self-standing carbon nitride films through the pyrolysis of a supramolecular hydrogel formed by hydrogen bonding between melamine and 4-cyanobenzoic acid. The self-standing filters show both good adsorption capability towards organic pollutants and good photocatalytic activity for the hydrogen evolution reaction. Such films were therefore employed as photoactive water-cleaning filters in a hybrid system performing both adsorption and photodegradation of two model pollutants in situ. The films display excellent stability and water cleaning performance after 10 consecutive cycles. We believe that this work opens the gate to sustainable low-weight metal-free membranes for environmental applications.

Experimental Section

Materials Synthesis

Melamine (1.26 g) and 4-cyanobenzoic acid (1.47 g) were dissolved separately, each in 100 mL of hot water (90 °C). The melamine solution was slowly added to the 4-cyanobenzoic acid solution, and the resulting mixture was kept at 90 °C for 3 h. A supramolecular hydrogel precursor was obtained after letting the solution cool to room temperature. The bulk precursor hydrogel was left to dry at room temperature and then heated (4 °C min^{-1}) to 500 °C, 550 °C, and 600 °C for 3 h under a N_2 atmosphere. The resulting carbon nitride self-standing materials were labelled as CBMA*xxx* (where *xxx* denotes the pyrolysis temperature).

For comparison, bulk carbon nitride (B-CN) was prepared by heating melamine at 4 °C/min to 550 °C and maintaining this temperature for 5 h. The resultant yellow material was milled to a fine powder using a mortar and pestle.

Materials Characterization

The Fourier transform infrared spectroscopy (FTIR) spectra were obtained using a Thermo Scientific Nicolet iN 10Mx infrared microscope. X-ray diffraction (XRD) patterns were obtained using an Empyrean powder diffractometer (Panalytical). Scanning electron microscopy (SEM) images were taken with a Thermo Fisher Verios 460L at 3 kV. Ultraviolet-visible spectroscopy (UV–vis) spectra were recorded using a Cary 100 spectrophotometer. X-ray photoelectron spectroscopy (XPS) was

performed in a Thermo Fisher Scientific ESCALAB 250 using monochromated Al Kα X-rays (1486.6 eV). Electrochemical measurements were recorded using a three-electrode system connected to an Autolab potentiostat (Metrohm, PGSTAT302N). A 1 cm^2 Pt-foil electrode and an Ag/AgCl (sat. KCl) electrode were used as the counter and reference electrodes, respectively. A Newport 300W Xe arc lamp equipped with air mass AM 1.5G and water filters were used as the light source. Mott–Schottky measurements were acquired in 0.2 M Na_2SO_4 solution to determine the flat band potentials of samples. Carrier density was estimated through Mott–Schottky relation:

$$1 / C_{sc}^2 = 2 (V - V_{fb} - K_b T / e) / (\varepsilon \varepsilon_0 A^2 e N_d) \quad (1)$$

where C_{sc} is the capacitance of the space charge region, e is the elementary charge of an electron (1.602×10^{-19} C), ε_0 is the permittivity of vacuum ($\varepsilon_0 = 8.854\times10^{-14}$ F cm^{-1}), ε is the dielectric constant of CN ($\varepsilon \approx 8$), A is the electrochemically active surface area, V is the applied voltage, V_{fb} is the flat-band potential, and N_d is the donor density. K_b and T represent Boltzmann's constant and temperature in K, respectively.

Adsorption performance

A 30 mg sample was added into a beaker containing 30 mL of an aqueous solution of MB with a concentration ranging from 0 to 10 mg L^{-1}. The suspension was then subjected to a 1 h magnetic stirring at 150 rpm and 288 K. After centrifugation, the dye solution concentration was determined by the UV–vis spectrophotometer.

The equilibrium adsorption amount was calculated according to the following equation:

$$q_e = (C_0 - C_e) V / m \quad (2)$$

where q_e (mg g^{-1}) is the equilibrium adsorption amount, C_0 (mg L^{-1}) is the initial concentration of the dye solution, C_e (mg L^{-1}) is the equilibrium concentration of the dye solution, V (L) is the volume of dye solution, and m (g) is the mass of the absorbent.

The adsorption isotherms were simulated following non-linear forms of Langmuir and Freundlich models:

$$q_e = (Q_0 b C_e) / (1 + b C_e) \quad (3)$$

$$q_e = k_F C_e^{(1/n)} \quad (4)$$

where q_e (mg g^{-1}) is the equilibrium adsorption amount, Q_0 (mg g^{-1}) is the maximum adsorption amount, b (L mg^{-1}) is a constant term related to the energy of adsorption, C_e (mg L^{-1}) is the equilibrium concentration of dye in the solution, k_F and n are the Freundlich constants, k_F represents the adsorption capacity of the adsorbent, and n indicates how favorable the adsorption process is (n = 2~10, 1~2, and < 1 indicate good, moderate, and poor adsorption, respectively).[59]

Photocatalytic activity

The photocatalytic activity was evaluated by carrying out the photodegradation of the MB dye under white-light irradiation (Bridge lux BXRA-50 C5300; λ> 410 nm). In a typical experiment, MB (20 mL, 10 mg L^{-1}) and the prepared material (20 mg) were mixed in a glass vial in the dark and under continuous stirring until an adsorption–desorption equilibrium was reached. After the light was turned on, aliquots were withdrawn at determined intervals, and the dye concentration was determined by UV–vis spectrophotometry. The kinetics of the photocatalytic degradation reaction were characterized by the following pseudo-first-order kinetic equation:

$$\ln (C/C_0) = - k t \quad (5)$$

where k is the apparent kinetic rate constant, C_0 and C are, respectively, the initial concentration at t = 0 and the instantaneous concentration of the MB solution at irradiation time t.

Hydrogen evolution measurements were performed in a previously reported setup,[34] using a Schlenk flask thermostatically controlled with a cooling system and a white LED array as the irradiation source. In a typical process, 15 mg of the carbon nitride sample was placed inside a 50 mL Schlenk flask containing 19 mL of a solvent mixture composed of water and TEOA in a 9:1 (v/v) ratio, and 19.6 µl of a H_2PtCl_6 solution, 8% in water (corresponding to a theoretical value of 3 wt% Pt loading onto the catalyst, total concentration of 0.207 mM); the temperature was maintained at 25 °C with a thermostat. The mixture was stirred for 30 min in the dark under a constant flow of argon, and the reaction was then started by switching on a 100 W (the illumination intensity on the photocatalyst surface is 10000 µmol s^{-1} m^{-2}) white LED array (Bridgelux BXRA-50C5300; λ > 410 nm). To confirm that the evolved gas was hydrogen, the headspace of the reactor was analyzed by Gas Chromatography (Agilent 7820 GC System).

Membrane filtration and photodegradation of pollutants from wastewater

Membrane flux was calculated by filtration time, effective area of membrane under the ambient pressure and room temperature. A schematic of the filtration setup is shown in Figure 4a. In a typical procedure, 5 mL of MB solution (20 mg L^{-1}) was added dropwise onto the surface of as-obtained membranes. Effective area of the membrane in the module was 2 cm^2. The fastest draining time of 5 mL MB aqueous solution was recorded to calculate the maximum water flux for filtration membranes. And the filtrate was sampled and analyzed by UV−vis spectroscopy to calculate the removal efficiency. The water permeation flux was calculated according to the following equation:

$$\text{Flux} = Q / (A \Delta t) \quad (6)$$

where Q is the quantity of permeate (L), i.e. 5 mL, A is the effective membrane area (m^2) and Δt is the draining time (h).[60]

The carbon nitride films were used as membranes for the removal of pollutants from wastewater by combining filtration and photodegradation. In a typical process, a 70 mg carbon nitride film was used as a filter membrane. A 20 mg L^{-1} MB (or RhB) aqueous solution was added dropwise (0.714 mL min^{-1}) to the filter membrane during 7 min, after which the filtrate was transferred into a UV–vis spectrophotometer cell to determine the dye concentration. The removal efficiency was calculated according to the following equation:

$$E = 100 * (C_1 - C_0) / C_0 \quad (7)$$

where E (%) is the removal efficiency, C_0 (mg L^{-1}) is the initial concentration of dye, C_1 (mg L^{-1}) is the concentration of filtrate.

To characterize the reusability and stability of the carbon nitride films, we conducted continuous degradation experiments. Every 7 min, the filtrate was transferred into a UV–vis spectrophotometer, where its dye concentration was determined.

Acknowledgements

This work was partially supported by the Israel Science Foundation, Grant No. 601/21, and ISF-NSFC Grant No. 2969/19. This project has received funding from the European Research Council (ERC) under the European Union's Horizon 2020 Research and Innovation Programme (Grant Agreement No. 849068). The authors thank Dr. Einat Nativ-Roth (IKI electron microscopy unit staff) for SEM measurements, and Dr. Jiawei Xia, Jonathan Tzadikov, Liel Abisdris, Rotem Geva, Ayelet Tashakory, Dr. Michael Volokh and Adi Azoulay (Ben-Gurion University of the Negev) for technical support. Junyi Li thanks the China Scholarships Council for its financial support.

Keywords: carbon nitride • supramolecular hydrogels • self-standing films • adsorption • photodegradation

References

[1] J. Mateo-Sagasta, S. M. Zadeh, H. Turral, **2018**.

[2] E. Obotey Ezugbe, S. Rathilal, *Membranes (Basel).* **2020**, *10*, 89.

[3] W. L. Ang, A. W. Mohammad, N. Hilal, C. P. Leo, *Desalination* **2015**, *363*, 2–18.

[4] A. Ejraei, M. A. Aroon, A. Ziarati Saravani, *J. Water Process Eng.* **2019**, *28*, 45–53.

[5] A. Bayat, S. F. Aghamiri, A. Moheb, G. R. Vakili‐Nezhaad, *Chem. Eng. Technol. Ind. Chem. Equipment‐Process Eng.* **2005**, *28*, 1525–1528.

[6] M. O. Adebajo, R. L. Frost, J. T. Kloprogge, O. Carmody, S. Kokot, *J. Porous Mater.* **2003**, *10*, 159–170.

[7] W. Lei, D. Portehault, D. Liu, S. Qin, Y. Chen, *Nat. Commun.* **2013**, *4*, 1777.

[8] C.-G. Lee, H. Javed, D. Zhang, J.-H. Kim, P. Westerhoff, Q. Li, P. J. J. Alvarez, *Environ. Sci. Technol.* **2018**, *52*, 4285–4293.

[9] M. Ateia, M. G. Alalm, D. Awfa, M. S. Johnson, C. Yoshimura, *Sci. Total Environ.* **2020**, *698*, 134197.

[10] M. K. Arfanis, P. Adamou, N. G. Moustakas, T. M. Triantis, A. G. Kontos, P. Falaras, *Chem. Eng. J.* **2017**, *310*, 525–536.

[11] J. Barrio, M. Volokh, M. Shalom, *J. Mater. Chem. A* **2020**, *8*, 11075–11116.

[12] V. W. Lau, B. V Lotsch, *Adv. Energy Mater.* **2022**, *12*, 2101078.

[13] W. J. Ong, L. L. Tan, Y. H. Ng, S. T. Yong, S. P. Chai, *Chem. Rev.* **2016**, *116*, 7159–7329.

[14] T. S. Miller, A. B. Jorge, T. M. Suter, A. Sella, F. Corà, P. F. McMillan, *Phys. Chem. Chem. Phys.* **2017**, *19*, 15613–15638.

[15] X. Wang, K. Maeda, A. Thomas, K. Takanabe, G. Xin, J. M. Carlsson, K. Domen, M. Antonietti, *Nat. Mater.* **2009**, *8*, 76–80.

[16] P. Niu, L. Zhang, G. Liu, H.-M. Cheng, *Adv. Funct. Mater.* **2012**, *22*, 4763–4770.

[17] L. Lin, Z. Yu, X. Wang, *Angew. Chemie - Int. Ed.* **2019**, *58*, 6164–6175.

[18] V. S. Vyas, F. Haase, L. Stegbauer, G. Savasci, F. Podjaski, C. Ochsenfeld, B. V Lotsch, *Nat. Commun.* **2015**, *6*, 8508.

[19] Y. Fang, X. Wang, *Chem. Commun.* **2018**, *54*, 5674–5687.

[20] J. Qin, S. Wang, H. Ren, Y. Hou, X. Wang, *Appl. Catal. B Environ.* **2015**, *179*, 1–8.

[21] J. Barrio, D. Mateo, J. Albero, H. García, M. Shalom, *Adv. Energy Mater.* **2019**, *9*, 1902738.

[22] P. Xia, M. Antonietti, B. Zhu, T. Heil, J. Yu, S. Cao, *Adv. Funct. Mater.* **2019**, *29*, 1–9.

[23] B. Kurpil, A. Savateev, V. Papaefthimiou, S. Zafeiratos, T. Heil, S. Özenler, D. Dontsova, M. Antonietti, *Appl. Catal. B Environ.* **2017**, *217*, 622–628.

[24] J. Wen, J. Xie, X. Chen, X. Li, *Appl. Surf. Sci.* **2017**, *391*, 72–123.

[25] Y. Fang, Y. Hou, X. Fu, X. Wang, *Chem. Rev.* **2022**, *122*, 4204–4256.

[26] S. Mazzanti, B. Kurpil, B. Pieber, M. Antonietti, A. Savateev, *Nat. Commun.* **2020**, *11*, 1387.

[27] I. Ghosh, J. Khamrai, A. Savateev, N. Shlapakov, M. Antonietti, B. König, *Science (80-.).* **2019**, *365*, 360 LP – 366.

[28] Y. Markushyna, C. A. Smith, A. Savateev, *European J. Org. Chem.* **2020**, *2020*, 1294–1309.

[29] S. Mazzanti, A. Savateev, *Chempluschem* **2020**, *85*, 2499–2517.

[30] L. Tian, J. Li, F. Liang, J. Wang, S. Li, H. Zhang, S. Zhang, *Appl. Catal. B Environ.* **2018**, *225*, 307–313.

[31] V. Hasija, P. Raizada, A. Sudhaik, K. Sharma, A. Kumar, P. Singh, S. B. Jonnalagadda, V. K. Thakur, *Appl. Mater. Today* **2019**, *15*, 494–524.

[32] G. Dong, Z. Ai, L. Zhang, *RSC Adv.* **2014**, *4*, 5553–5560.

[33] C. Jia, L. Yang, Y. Zhang, X. Zhang, K. Xiao, J. Xu, J. Liu, *ACS Appl. Mater. Interfaces* **2020**, *12*, 53571–53591.

[34] J. Barrio, M. Shalom, *ACS Appl. Mater. Interfaces* **2018**, *10*, 39688–39694.

[35] M. Volokh, G. Peng, J. Barrio, M. Shalom, *Angew. Chemie - Int. Ed.* **2019**, *58*, 6138–6151.

[36] W. Xiong, F. Huang, R.-Q. Zhang, *Sustain. Energy Fuels* **2020**, DOI 10.1039/C9SE00785G.

[37] K. Xiao, P. Giusto, L. Wen, L. Jiang, M. Antonietti, *Angew. Chemie - Int. Ed.* **2018**, 57, 10123–10126.

[38] K. Xiao, L. Chen, R. Chen, T. Heil, S. D. C. Lemus, F. Fan, L. Wen, L. Jiang, M. Antonietti, *Nat. Commun.* **2019**, 10, DOI 10.1038/s41467-018-08029-5.

[39] Q. Cao, B. Kumru, M. Antonietti, B. V. K. J. Schmidt, *Mater. Horizons* **2020**, *7*, 762–786.

[40] B. Kumru, J. Barrio, J. Zhang, M. Antonietti, M. Shalom, B. V. K. J. Schmidt, *ACS Appl. Mater. Interfaces* **2019**, *11*, 9462–9469.

[41] H. Lan, F. Wang, M. Lan, X. An, H. Liu, J. Qu, *Environ. Sci. Technol.* **2019**, 53, 6981–6988.

[42] A. Castiñeiras, I. García-Santos, J. M. González-Pérez, A. Bauzá, J. K. Zaręba, J. Niclós-Gutiérrez, R. Torres, E. Vílchez, A. Frontera, *Cryst. Growth Des.* **2018**, *18*, 6786–6800.

[43] A. Saha, B. Roy, A. Garai, A. K. Nandi, *Langmuir* **2009**, *25*, 8457–8461.

[44] P. Meng, Y. Xu, C. Yan, J. Xu, *ACS Appl. Mater. Interfaces* **2020**, *12*, 53125–53133.

[45] J. Barrio, M. Shalom, *ChemCatChem* **2018**, *10*, 5573–5586.

[46] B. Roy, P. Bairi, A. K. Nandi, *RSC Adv.* **2014**, *4*, 1708–1734.

[47] X. Han, L. Tian, H. Jiang, L. Kong, J. Lv, J. Shan, J. Wang, X. Fan, *RSC Adv.* **2017**, *7*, 14372–14381.

[48] J. Liu, T. Zhang, Z. Wang, G. Dawson, W. Chen, *J. Mater. Chem.* **2011**, *21*, 14398–14401.

[49] J. Li, X. Wang, L. Huang, L. Tian, M. Shalom, C. Xiong, H. Zhang, Q. Jia, S. Zhang, F. Liang, *Nanoscale* **2021**, *13*, 12634–12641.

[50] W. Shipeng, O. Man, Z. Qin, Z. Shule, C. Wei, *Adv. Opt. Mater.* **2017**, *5*, 1700536.

[51] J. Barrio, S. Barzilai, N. Karjule, P. Amo‐Ochoa, F. Zamora, M. Shalom, *Adv. Opt. Mater.* **2021**, *9*, 2100683.

[52] Z. Zhou, F. He, Y. Shen, X. Chen, Y. Yang, S. Liu, T. Mori, Y. Zhang, *Chem. Commun.* **2017**, *53*, 2044–2047.

[53] J. Li, N. Karjule, J. Qin, Y. Wang, J. Barrio, M. Shalom, *Molecules* **2021**, *26(6)*, 1646.

[54] S. C. Karunakaran, B. J. Cafferty, K. S. Jain, G. B. Schuster, N. V. Hud, *ACS Omega* **2020**, *5*, 344–349.

[55] J. Xu, G. Wu, Z. Wang, X. Zhang, *Chem. Sci.* **2012**, *3*, 3227–3230.

[56] G. Zhang, J. Zhang, M. Zhang, X. Wang, *J. Mater. Chem.* **2012**, *22*, 8083–8091.

[57] X. Li, J. Wang, J. Xia, Y. Fang, Y. Hou, X. Fu, M. Shalom, X. Wang, ChemSusChem **2022**, 15, 1–6.

[58] X. Li, X. Chen, Y. Fang, W. Lin, Y. Hou, M. Anpo, X. Fu, X. Wang, Chem. Sci. **2022**, 7541–7551.

[59] L. Tian, F. Liang, L. Dong, J. Li, Q. Jia, H. Zhang, S. Yan, S. Zhang, *J. Am. Ceram. Soc.* **2021**, *104*, 1110–1119.

[60] E. Saljoughi, M. Sadrzadeh, T. Mohammadi, *J. Memb. Sci.* **2009**, 326, 627–634.

Entry for the Table of Contents

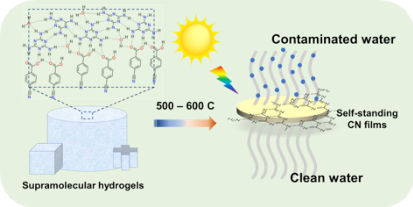

Self-standing carbon nitride films were prepared by drying and calcinating tailored supramolecular hydrogels composed of melamine and 4-cyanobenzoic acid. The resulting self-standing films were employed as filters combining adsorption and photodegradation of organic pollutants showing remarkable activity and stability in flow conditions.

Chemistry–A European Journal

Supporting Information

Efficient Water Cleaning by Self-standing Carbon Nitride Films Derived from Supramolecular Hydrogels

Junyi Li, Snir Dor, Jesús Barrio,* and Menny Shalom*

Table S1 Elemental analysis of as-obtained samples.

	CBMA500	CBMA550	CBMA600
C (at%)	33.7	40.7	47.6
N (at%)	36.2	35.6	32.8
H (at%)	25.9	20.3	17.2
O (at%)	4.2	3.4	2.4
C/N ratios	0.93	1.14	1.45

Table S2 Adsorption kinetic parameters calculated based on Eqs. (2) and (3).

Sample	Freundlich			Langmuir		
	k_F	n	R^2	Q_0	b	R^2
B-CN	0.45	2.46	0.98	1.32	0.43	0.97
CBMA500	1.15	3.71	0.87	2.11	1.21	0.99
CBMA550	1.3	3.21	0.92	2.61	1.01	0.99
CBMA600	1.41	2.67	0.97	3.28	0.75	0.99

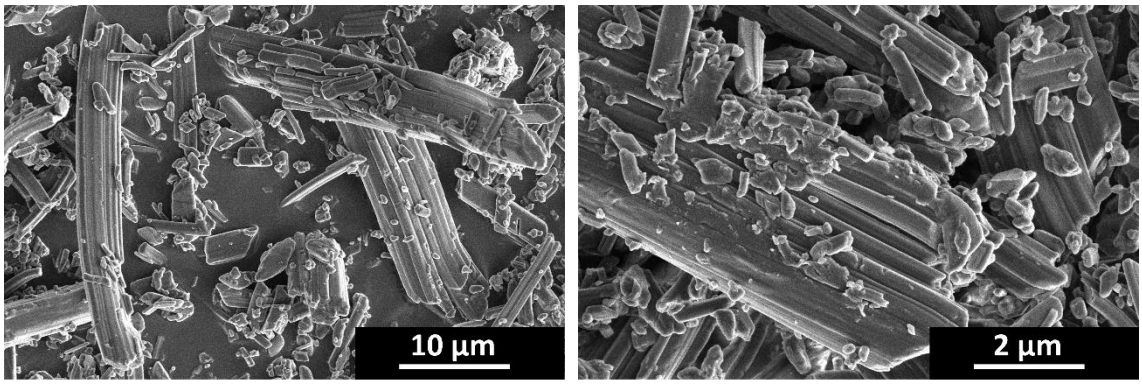

Figure S1. SEM images of supramolecular precursor. (CB/MA ratio = 1:1)

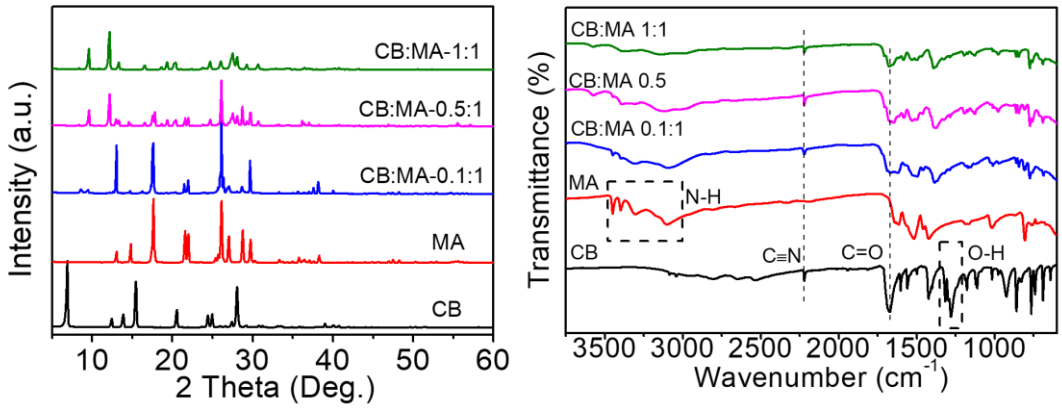

Figure S2. XRD patterns and FTIR spectra of supramolecular precursors with different CB/MA ratios.

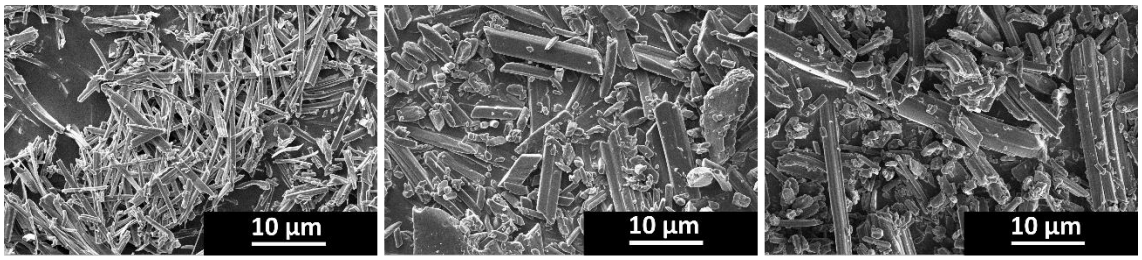

Figure S3. SEM images of supramolecular precursors with different CB/MA ratios.

(The CB/MA ratios are 0.1:1, 0.5:1, and 1:1 from left to right)

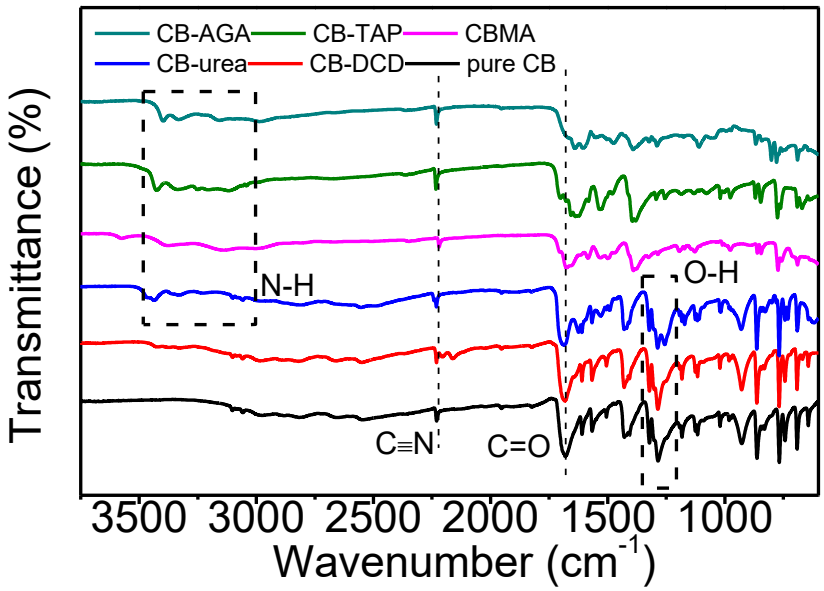

Figure S4. FTIR spectra of different supramolecular precursors of hydrogels incorporating CB.

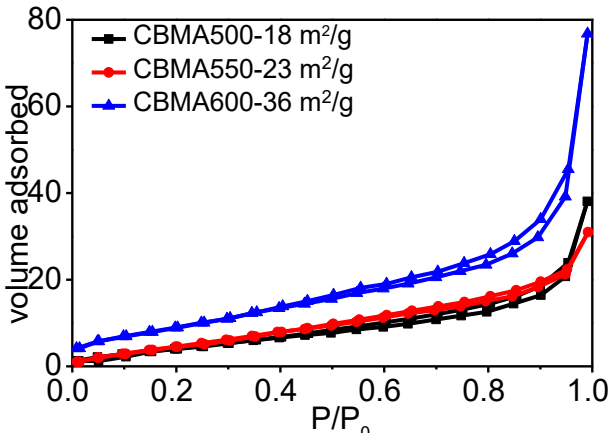

Figure S5. N_2 adsorption and desorption isotherms of as-obtained CBMA samples.

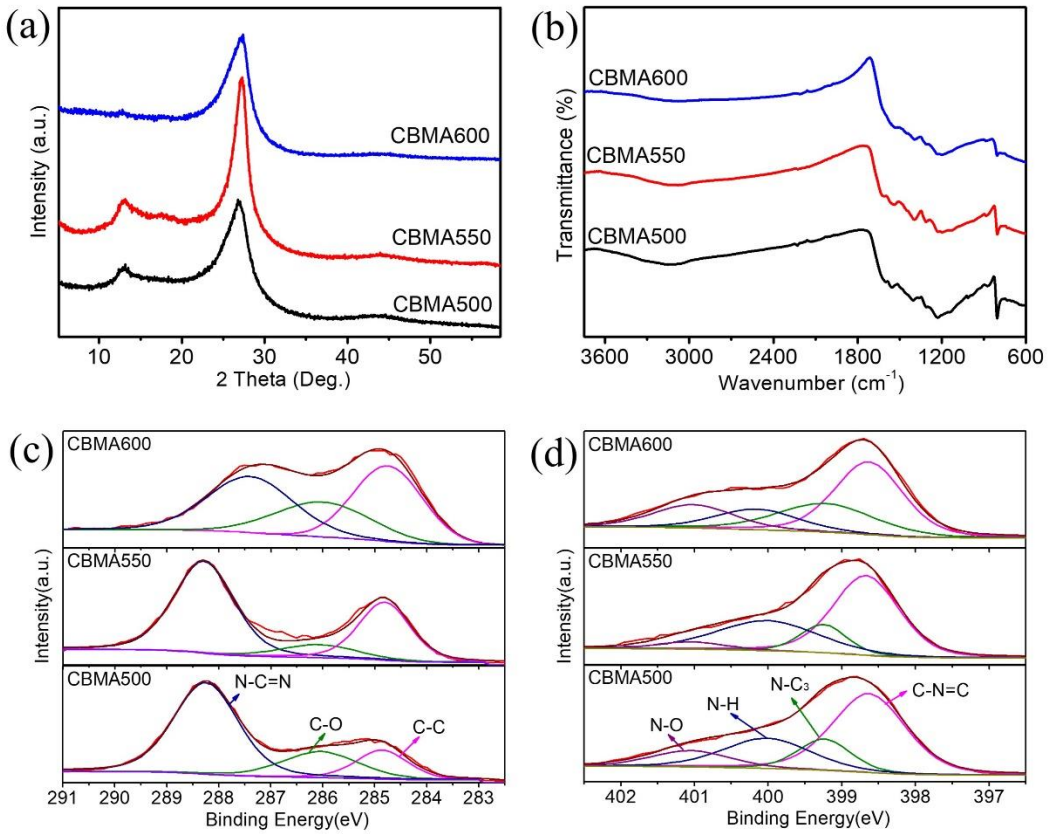

Figure S6. (a) XRD patterns, (b) FTIR spectra, (c) high-resolution C 1s XPS spectra, and (d) high-resolution N 1s spectra of as-obtained CBMA samples.

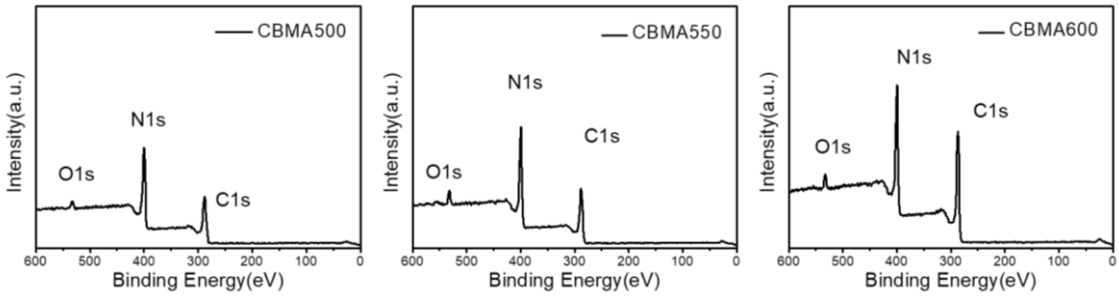

Fig. S7 XPS wide spectra of as-obtained CBMA samples.

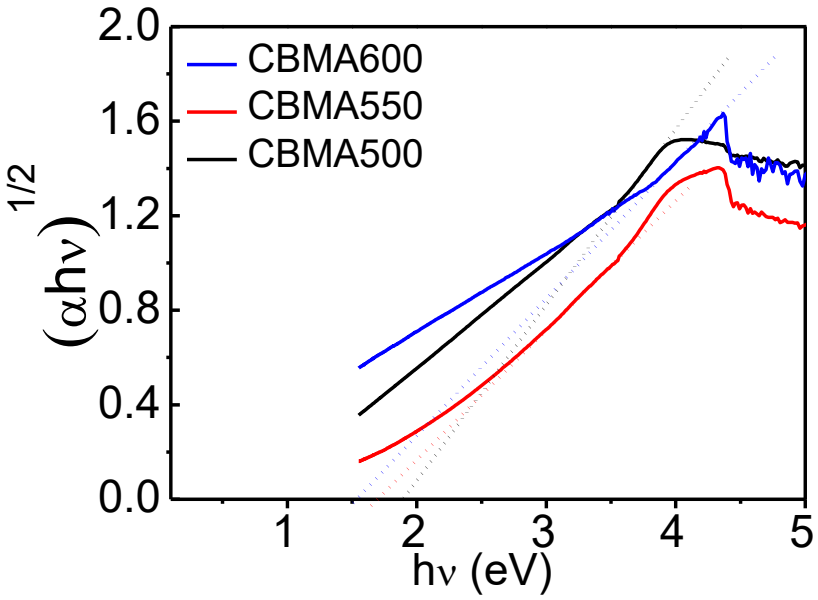

Figure S8. Tauc plots of as-obtained CBMA samples.

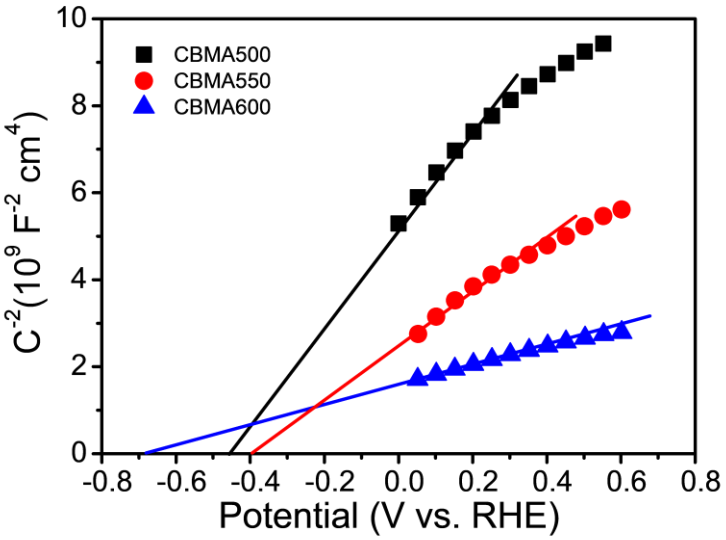

Figure S9. Mott–Schottky plots of as-obtained CBMA samples to measure the flat-band potentials.

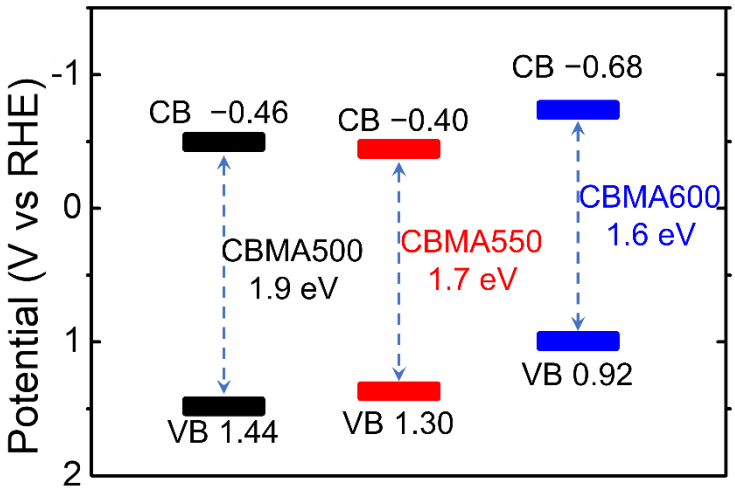

Figure S10. Band structure of as-obtained CBMA samples.

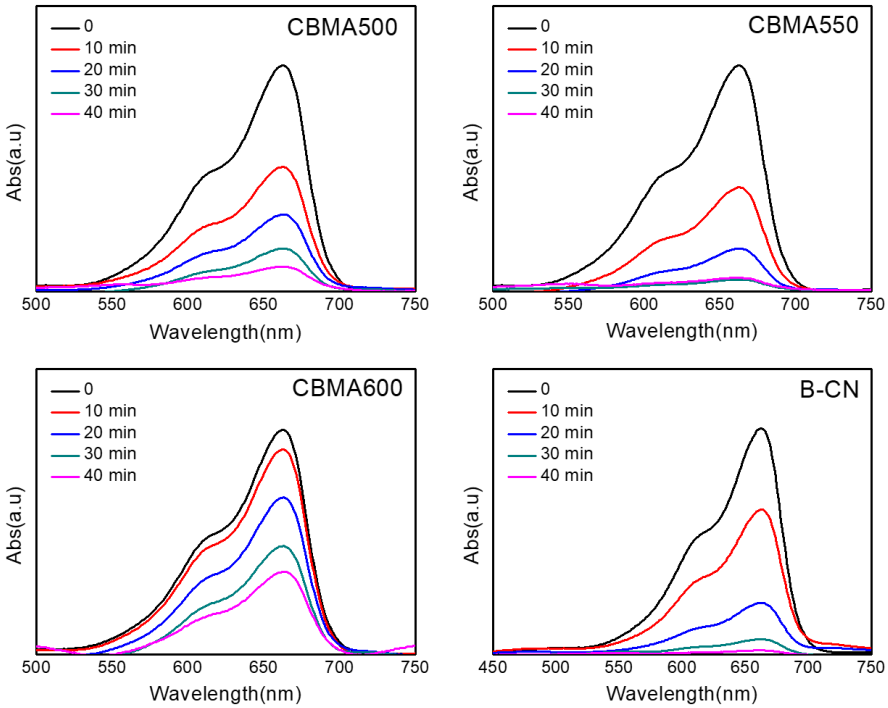

Figure S11. UV-vis absorption spectra of a methylene blue solution under visible light irradiation (λ > 410 nm) after different times over: (a) CBMA500, (b) CBMA550, (c) CBMA600, and (d) B-CN.

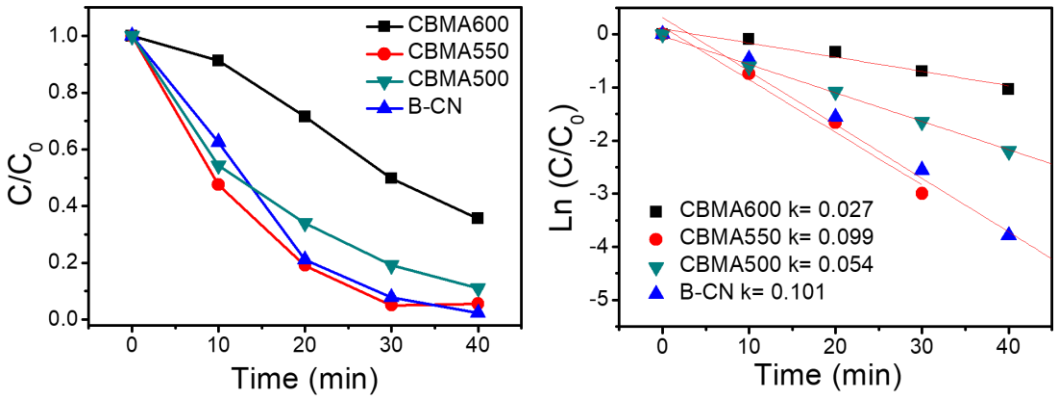

Figure S12. Relative concentration of RhB (left) and its natural logarithm (right) as a function of illumination time in the presence of various carbon nitride materials.

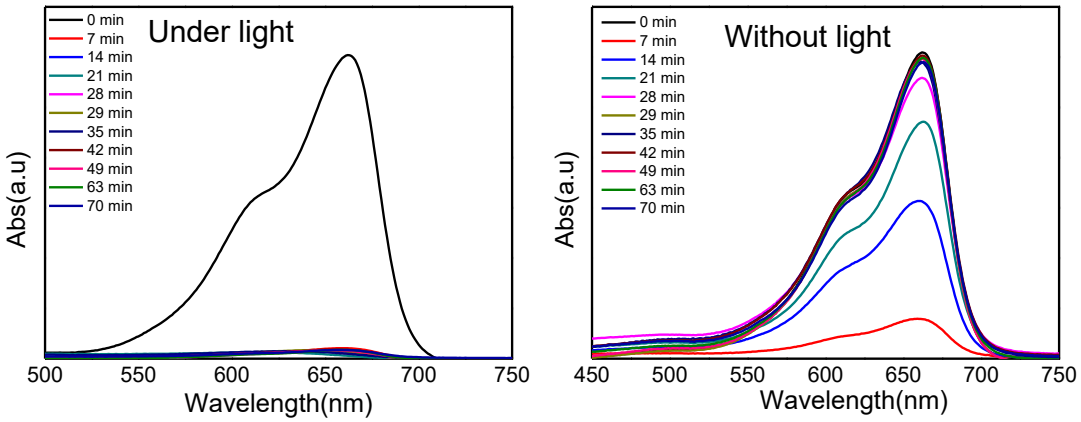

Figure S13. UV-vis absorbance spectra of a filtrate of an MB solution passed through a CBMA550 filter under light (left) and without light (right).